Chemistry–A European Journal
Research Article
doi.org/10.1002/chem.202302148
Chemistry Europe
European Chemical Societies Publishing
www.chemeurj.org

Synthesis, Structure, and Redox and Optical Properties of 5,10,15,20-Tetraaryl-5-azaporphyrinium Salts

Yuta Kudoh,[b] Emi Suzuki,[b] Hikari Ochiai,[b] Kakeru Ise,[c] Yoshifumi Kimura,[c] Mao Minoura,[d] Haruyuki Nakano,[e] and Yoshihiro Matano*[a]

The fundamental properties of azaporphyrins can be modulated over a wide range by changing the number of *meso*-nitrogen atoms. Reported herein are the first examples of 5,10,15,20-tetraaryl-5-azaporphyrinium (MTAMAP) salts, which were prepared via metal-templated cyclization of the corresponding zinc(II) and copper(II) complexes of 10-aryl-1-chloro-19-benzoyl-5,15-dimesityl-10-azabiladiene-*ac*. The inclusion of one *meso*-nitrogen atom in the 5,10,15,20-tetraarylporphyrin skeleton considerably changes the redox and optical properties as well as the degree of aromaticity of the porphyrin ring. The present findings suggest that MTAMAP salts would be promising scaffolds for the development of new azaporphyrin-based ionic fluorophores and photosensitizers.

Introduction

Diversification of the redox and optical properties of porphyrin is a significant challenge in the further development of porphyrin-based materials and catalysts. Thus, azaporphyrins have attracted considerable attention because their structures and fundamental properties can be modulated over a wide range by changing the number of *meso*-nitrogen atoms.[1] The energy gaps between the highest occupied molecular orbital (HOMO) and lowest unoccupied molecular orbital (LUMO) of azaporphyrins decreases with an increase in the number of *meso*-nitrogen atoms, resulting in a gradual red shift and intensification of the Q band.[2] In addition to well-developed phthalocyanines, 5,15-diazaporphyrins (DAPs) are the most extensively studied azaporphyrins and their potential as photosensitizers[3,4] and catalysts[5] has been highlighted in recent years. For example, peripherally functionalized DAPs exhibit high $^1O_2$-generation efficiencies in response to long-wavelength visible light and are currently being investigated for use in photodynamic therapy (PDT).[3] Recently, we reported redox-switchable 5,10,15,20-tetraaryl-5,15-diazaporphyrinoid (TADAP; **P1**) as a new family of DAP (Figure 1).[6] Notably, TADAPs with the 20π- or 19π-electron circuit are extremely air-stable compared with isoelectronic 5,10,15,20-tetraarylporphyrin (TAP) anions owing to the inclusion of two *meso*-N atoms in the porphyrin ring of the former, which induces pronounced anodic shifts of the 18π/19π- and 19π/20π-electron redox couples. This property of TADAP was found to be effective in conferring stability to DAP-based electrochromic materials[7] and metal catalysts.[8] In addition, the highly flat 20π-electron ring of TADAP is convenient for assessing antiaromaticity owing

[a] *Prof. Dr. Y. Matano*
Department of Chemistry, Faculty of Science
Niigata University
Nishi-ku, Niigata 950-2181 (Japan)
E-mail: matano@chem.sc.niigata-u.ac.jp
[b] *Y. Kudoh, E. Suzuki, H. Ochiai*
Department of Fundamental Sciences
Graduate School of Science and Technology
Niigata University
Nishi-ku, Niigata 950-2181 (Japan)
[c] *K. Ise, Prof. Dr. Y. Kimura*
Department of Applied Chemistry
Graduate School of Science and Engineering
Doshisha University
Kyotanabe, 610-0321 (Japan)
[d] *Prof. Dr. M. Minoura*
Department of Chemistry, College of Science
Rikkyo University, Toshima-ku, Tokyo 171-8501 (Japan)
[e] *Prof. Dr. H. Nakano*
Department of Chemistry
Graduate School of Science
Kyushu University
Nishi-ku, Fukuoka 819-0395 (Japan)

Supporting information for this article is available on the WWW under https://doi.org/10.1002/chem.202302148

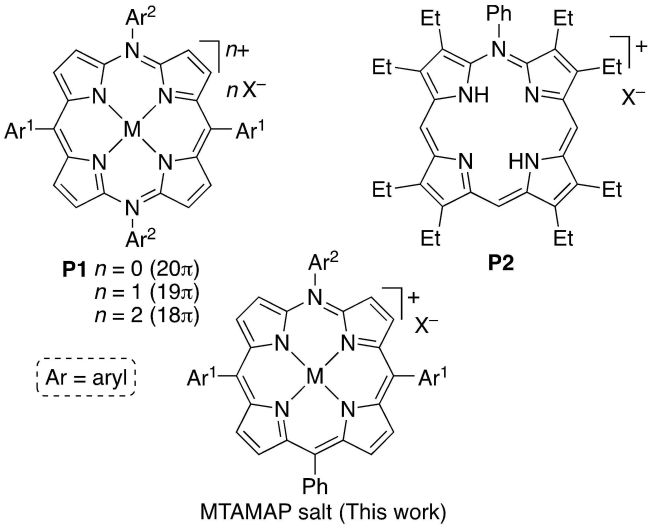

Figure 1. Structures of *meso*-N-substituted azaporphyrins. MTADAP **P1** (M = metal or H_2), β-substituted MAP salt **P2**, and MTAMAP salt (M = Zn, Cu, or H_2).

to the absence of undesired ring-distortion effects,[9] which are unavoidable in isoelectronic TAPs.

In contrast to DAPs, 5-monoazaporphyrins (MAPs) have received little attention and their structure-property relationships have not been fully elucidated.[10–12] Recently, Shinokubo and Takiguchi reported the free base of 2,3,7,8,12,13,17,18-octaethyl-5-azaporphyrinium salt **P2** as the first example of a MAP bearing a substituent on the *meso*-N atom, which can be obtained from the corresponding 5-oxaporphyrinium ion[13] via sequential ring-opening and -closing reactions.[14] However, there is no report on the synthesis of MAPs bearing four *meso*-substituents. We hypothesized that including one *meso*-N atom in the TAP ring would result in a charge shift of +1 and thus redox and optical properties that differ from those of TADAP. Herein, we report the first examples of zinc(II) and copper(II) complexes and the free base of 5,10,15,20-tetraaryl-5-azaporphyrinium salts (MTAMAP salts; M = Zn, Cu, H_2), along with their structure-property relationships.

Results and Discussion

Scheme 1 depicts the synthesis of MTAMAP salts. The addition of 1,3-dichloro-5,5-dimethylhydantoin (DCDMH) to a THF solution of 1-benzoyl-5-mesityldipyrromethane **1**, obtained by benzoylation of 5-mesityldipyrromethane according to Lindsey's method[15] (see, the Supporting Information), followed by treatment with 2,3-dichloro-5,6-dicyano-1,4-benzoquinone (DDQ) at −78 °C afforded 1-benzoyl-9-chloro-5-mesityldipyrrin **2** (mesityl = 2,4,6-trimethylphenyl). Sequential treatment of zinc(II) acetate with **2** and 1-arylamino-9-bromo-5-mesityldipyrrin **3a** in the presence of 1,8-diazabicyclo[5.4.0]-7-undecene (DBU) in CH_2Cl_2-MeOH produced a mixture of zinc(II)-bis(dipyrrin) complexes including **4a**, which was heated with Cs_2CO_3 in *N*,*N*-dimethylformamide (DMF) at 110 °C to afford the zinc(II) complex of 10-aryl-1-bromo-19-benzoyl-5,15-dimesityl-10-azabiladiene-*ac* **5a** after chromatographic separation. Similar sequential reactions of zinc(II) acetate with **2**/**3b** and **2**/**3c** yielded corresponding zinc(II) complexes **5b** and **5c**, respectively. Metal-templated C–C-bond-forming annulation of **5** in the presence of excess $NaBH_4$ in 2-propanol at 80 °C afforded corresponding ZnTAMAP salts, which were isolated as chlorides **6-Cl** by treatment with NaCl.

Metathesis of **6a-Cl** with $AgPF_6$ and $AgNTf_2$ in CH_2Cl_2 furnished **6a-PF$_6$** and **6a-NTf$_2$**, respectively. Demetallation of **5a,c** with trifluoroacetic acid afforded free bases **7a,c**, which were converted to corresponding copper(II) complexes **8a,c** by metallation with copper(II) acetate in CH_2Cl_2–MeOH. Metal-templated annulation of **8a,c** with $NaBH_4$ followed by anion exchange with KPF_6 yielded CuTAMAP salts **9a,c-PF$_6$**. Treatment of ZnTAMAP salt **6a-Cl** with excess Me_3SiBr in the presence of a small amount of MeOH in CH_2Cl_2 at room temperature yielded H_2TAMAP salt **10a-Br**, which was further converted to **10a-PF$_6$** by treatment with KPF_6 (Scheme 2).[16] Complexation of free base **10a-PF$_6$** with copper(II) acetate in CH_3CN proceeded smoothly to afford **9a-PF$_6$** after anion exchange with KPF_6.

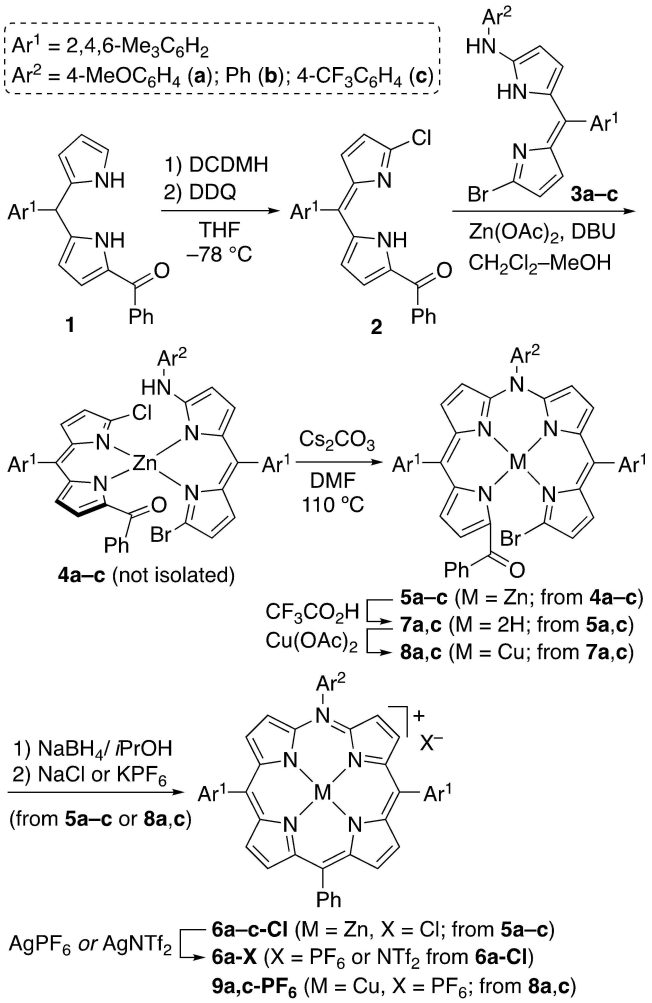

Scheme 1. Synthesis of MTAMAP salts **6-X** and **9-PF$_6$**.

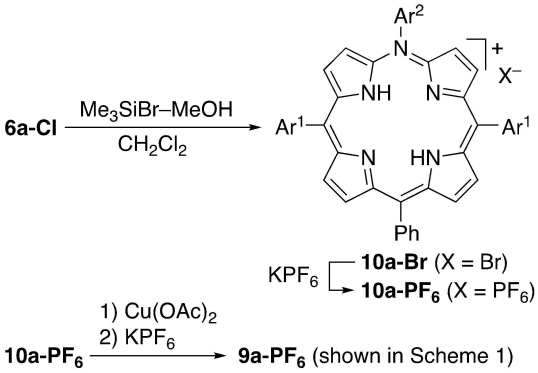

Scheme 2. Synthesis of H_2TAMAP salts **10a-X** and CuTAMAP salt **9a-PF$_6$**.

MTAMAP salts were characterized using NMR and IR spectroscopy, high-resolution mass (HRMS) spectrometry, and X-ray crystallography. The HRMS spectra of the MTAMAP salts contained intense peaks corresponding to $[M–X]^+$ fragment ions. The $^{31}P\{^1H\}$ and $^{19}F\{^1H\}$ NMR spectra of **6-PF$_6$**, **6a-NTf$_2$**, and **10a-PF$_6$** contained characteristic signals derived from the counter anions. In the ^1H NMR spectra of **6-X** and **10a-X** in

$CDCl_3$, the pyrrolic β-protons appeared as four doublet signals in the range of 8.6–7.5 ppm, reflecting diatropic ring-current effects from their 18π-electron circuits. The aromatic character of the ZnTAMAP cation was evaluated on the basis of the nucleus-independent chemical shift (NICS)[17] of their models (Figure S1a in the Supporting Information). The NICS(0) values at the midpoints between the two adjacent pyrrole rings of ZnTAMAP cation (**6m**$^+$; −10.9 to −8.3 ppm) were less negative than those of zinc(II) complex of 5,10,15,20-tetraphenylporphyrin (ZnTPP; −18.8 ppm) and ZnTADAP dication (**Zn-P1 m**$^{2+}$; −17.7 to −17.1 ppm), indicating that the ring-current effects of the ZnTAMAP cation were weaker than those of the isoelectronic ZnTPP and ZnTADAP dication. This was further supported by the anisotropy of the current-induced density (ACID) analysis of (aza)porphines.[18] Specifically, the current density vectors plotted on the ACID isosurface in 5-HMAP$^+$ were fewer than those in porphine and 5,15-H_2DAP^{2+} (Figure S2). The relatively weaker aromaticity of 5-HMAP$^+$ is attributable to its highly polarized structure,[19] which may reduce the efficiency of the global π-electron delocalization in the MAP ring.[20] The NH signal of **10a-PF$_6$** (0.74 ppm) was less shielded than the NH signal of **P1** (−0.54 ppm; M = H_2; X = PF_6), which clearly reflected the relatively weak ring-current effect of the H_2MAP ring. This was also supported by the NICS(0) values calculated at the macrocyclic center of the corresponding models and free base TPP (H_2TPP); −6.8 ppm for **10m**$^+$, −13.9 ppm for **H_2-P1 m**$^{2+}$, and −15.6 ppm for H_2TPP (Figure S1b).

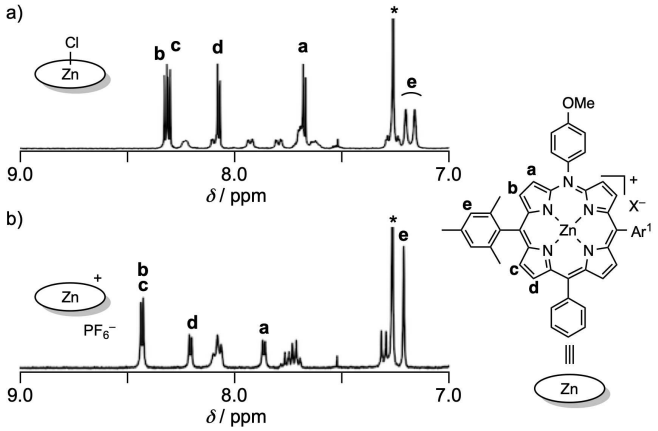

Figure 2. ^{1}H NMR spectra (400 MHz, $CDCl_3$; δ 9-7) of a) **6a-Cl** and b) **6a-PF$_6$**. Asterisk indicates a signal of residual $CHCl_3$.

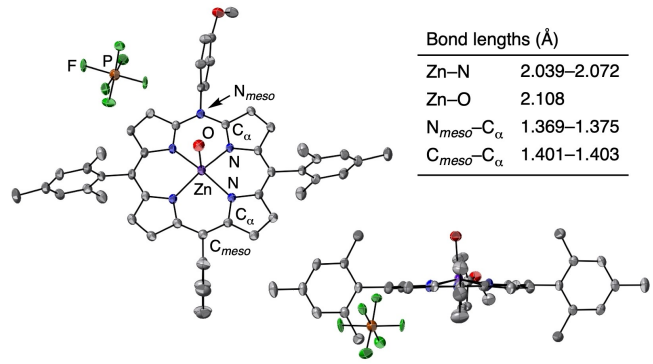

Figure 3. ORTEP diagrams (50% probability ellipsoids) of **6a-PF$_6$**·H_2O. Hydrogen atoms are omitted for clarity. Selected bond lengths (Å), except the standard deviations (0.002-0.004 A), are shown.

In the ^{1}H NMR spectra of **6a-X** in $CDCl_3$, the *ortho*-CH_3/*meta*-H signals of the mesityl groups were nonequivalent for **6a-Cl** but equivalent for **6a-PF$_6$** (Figure 2). These spectral features indicated that the chloride ion of **6a-Cl** was tightly bound to its zinc center to form a pentacoordinate zinc(II) complex. In contrast, there was little difference between the ^{1}H NMR spectra of **6a-Cl** and **6a-PF$_6$** in CD_3OD, suggesting that the ZnTAMAP cation and counter anions were efficiently solvated in this protic polar solvent (Figure S3). The ^{1}H NMR spectra of **10a-X** (X = Br, PF_6) in $CDCl_3$ were similar (Figure S4).

Figures 3 and S5 show the X-ray crystal structure and bond parameters of **6a-PF$_6$**·H_2O. The zinc center had a square pyramid geometry and deviated from the core-N_4 plane by 0.375 Å owing to the axial coordination of the H_2O molecule.[21] The MAP ligand was highly planar with a root-mean-square deviation of 0.046 Å. The *meso*-aryl groups were almost perpendicular to the MAP ring (dihedral angles are 83.6–88.4°), suggesting that π-conjugation between the *meso*-aryl groups and the MAP ring was minimal. The N_{meso}–C_α bond lengths (1.369–1.375 Å) were appreciably shorter than the C_{meso}–C_α bond lengths (1.401–1.403 Å). Table S1 shows the bond parameters of **6a-PF$_6$**·H_2O together with those of porphyrin models calculated by density functional theory (DFT). The difference in the C–C/C–N bond lengths among **6a-PF$_6$**·H_2O, **6m**$^+$, and **6m-Cl** was insignificant, which suggested that the axial ligand had little effect on the degree of the π-conjugation of the ZnMAP ring. The harmonic oscillator model of aromaticity (HOMA)[22] value of **6a-PF$_6$**·H_2O (0.692) determined using the 18 C–C/C–N bonds constituting the 18π-electron circuit was comparable with that of **6m**$^+$ (0.693) but was smaller than that of ZnTPP (0.712). These data support the relatively weak aromatic character of the MAP ring of **6-X** in terms of the geometrical criterion.

The UV/vis absorption and emission spectra of **6-X**, **9-PF$_6$**, and **10a-X** are shown in Figures 4 and S6, and their optical data are summarized in Table 1. The spectral shapes and absorption maxima (λ_{ab}) of **6-X** in CH_2Cl_2 varied slightly depending on the counter anions, whereas those of **6-X** in MeOH were almost the same. All the MTAMAP salts exhibited Q-like bands, and the λ_Q value of **6b-Cl** (615 nm) was significantly red-shifted compared with that of ZnTAP with the same *meso*-substituents (λ_Q = 551 nm).[6b] The observed absorption bands of **6-X** were assigned using time-dependent DFT (TD-DFT) calculations, which revealed that the axial coordination of the chloride ion had little impact on the HOMO-to-LUMO π-π* transition energy of the cationic TAMAP chromophore (Table S2). Both **6-X** and **10a-X** emitted fluorescence with emission maxima (λ_{em}) of 616–629 nm and quantum yields (Φ_{em}) of 0.068–0.197. From these data, the lowest excited singlet-state energies of **6-X** and **10a-X** were determined to be 2.00–2.02 eV. Notably, the fluorescence intensities of ZnTAMAP salts **6-X** were dependent on the counter anions and solvents: In CH_2Cl_2, the Φ_f value of **6a-Cl** (0.069) was smaller than that of **6a-NTf$_2$** (0.106), whereas, in MeOH, the Φ_f values of **6a-Cl** and **6a-NTf$_2$** were comparable

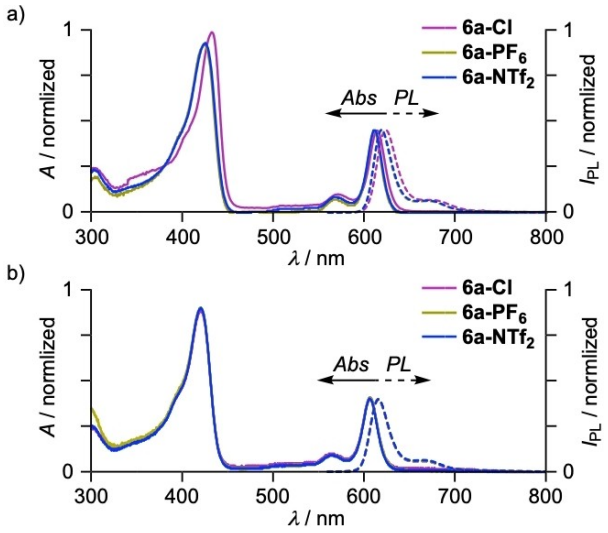

Figure 4. UV/vis absorption and emission spectra of **6a-X** in a) CH_2Cl_2 and b) MeOH.

Table 1. Optical data and redox potentials of MTAMAP salts.[a]

TAMAP	λ_{abs} [nm] [b]	λ_{em} [nm][c] (Φ_{em})[d]	$E_{1/2}$ [V][e]
6a-Cl	433, 571, 614	623 (0.069)	−1.24, +0.75
6a-Cl [f]	421, 565, 608	616 (0.095)	N.m.
6a-PF_6	424, 567, 610	618 (0.075)	N.m.
6a-PF_6 [f]	421, 566, 608	616 (0.087)	N.m.
6a-NTf_2	424, 568, 610	618 (0.106)	N.m.
6a-NTf_2 [f]	421, 565, 607	616 (0.102)	N.m.
6b-Cl	432, 572, 615	625 (0.085)	−1.08, +0.93
6c-Cl	433, 574, 617	629 (0.068)	−1.02, +1.01
9a-PF_6	413, 566, 609	827 (< 0.003)	−1.54, −0.93, +1.10
9c-PF_6	412, 569, 613	830 (< 0.003)	−1.36, −0.87, +1.14
10a-Br	411, 570, 620	626 (0.183)	N.m.
10a-PF_6	411, 570, 621	626 (0.197)	−1.49, −0.83, +1.23

[a] Measured in CH_2Cl_2 unless otherwise noted. N.m. = Not measured. [b] Absorption maxima; > 400 nm). Molecular absorption coefficients are reported in SI. [c] Emission maxima: λ_{ex} = 421–433 nm (**6a-X**); 433 nm (**6b-Cl**); 433 nm (**6c-Cl**); 613 nm (**9a-X**); 411 nm (**10a-X**). [d] Absolute emission quantum yields: λ_{ex} = 420 nm (**6a-X**, **6b-Cl**); 410 nm (**6c-Cl**, **9-PF_6**, **10a-Br**); 400 nm (**10a-PF_6**). [e] Half-wave potential of 19π/18π- and 18π/17π-electron redox couples. [f] Measured in MeOH.

(0.095–0.102). The ZnTAMAP cation and chloride ion of **6a-Cl** were likely present as a tightly ion-paired 5-coordinate complex in CH_2Cl_2 and a solvent-separated ion pair in MeOH, as suggested by the ^{1}H NMR spectra. The counter anions of H_2TAMAP salts **10a-X** had a minor effect on the absorption and emission spectra of the salts in CH_2Cl_2.

In contrast to **6-PF_6** and **10a-X**, CuTAMAP salts **9-PF_6** emitted phosphorescence in CH_2Cl_2 with λ_{em} of 827–830 nm at room temperature under an Ar atmosphere (Figure S6), although their quantum yields were low (Φ_{em} < 0.003). The lowest triplet-state energies of **9-PF_6** calculated from the λ_{em} were 1.49–1.50 eV.

To gain further insight into the excited-state dynamics of ZnTAMAP salts, we measured the fluorescence lifetimes (τ_f) of **6a-X** in solution (Table S3). The radiative and nonradiative rate constants (k_f and k_{nr}) obtained from the τ_f and Φ_f values are summarized in Table S3. The fluorescence decay profiles of **6a-PF_6** and **6a-NTf_2** were analyzed, revealing that these compounds existed as a single component, which suggested that the soft anions (PF_6^- and NTf_2^-) did not interact with the TAMAP cation in the excited state. In contrast, **6a-Cl** exhibited solvent-dependent decay profiles. Specifically, **6a-Cl** existed as a single component in MeOH but as a binary component in CH_2Cl_2. For **6a-Cl** in CH_2Cl_2, an equilibrium might exist between the contact ion pair and the solvent-separated ion pair in the excited state, and the former showed the faster fluorescence decay.

We next measured the redox potentials of MTAMAP salts in CH_2Cl_2 with Bu_4NPF_6 as a supporting electrolyte (Figures 5 and S7 and Table 1). Reversible waves corresponding to the 19π/18π- and 18π/17π-electron redox processes were observed with the half-wave potentials ($E_{1/2}$) of −0.83 to −1.24 V and +0.75 to +1.23 V vs. the ferrocene/ferrocenium couple (Fc/Fc^+), respectively. The 19π/18π redox process shifted to the positive side in the order Zn-porphyrin ($E_{1/2}$ = −1.97 V),[23] **6b-Cl** ($E_{1/2}$ = −1.08 V), and **P1** (M = Zn, Ar = Ph; $E_{1/2}$ = −0.18 V). The 18π/17π redox process also shifted similarly. These results indicate that the charge of the 18π-electron (aza)porphyrin ring, from 0 to +1 to +2, lowers the LUMO and HOMO levels step by step. This is consistent with the energy gaps of their models predicted by DFT calculations (Figure S1). The electronic effect of the *para* substituents on the redox potentials was small but distinct. Specifically, the $E_{1/2}$ values slightly shifted to the positive side in the order **6a**, **6b**, and **6c**. The CuTAMAP cation **9a$^+$** showed redox processes at the more positive potentials than those of the ZnTAMAP cation **6a$^+$**, which reflected the difference in electronegativities of the central metals (1.65 for Zn, 1.90 for Cu; Pauling scale). The copper complexes **9a-PF_6** and **9c-PF_6** and free base **10a-PF_6** showed additional waves corresponding to the 20π/19π redox couple. For all the 18π-electron MTADAP salts, the electrochemical HOMO-LUMO gaps were in good

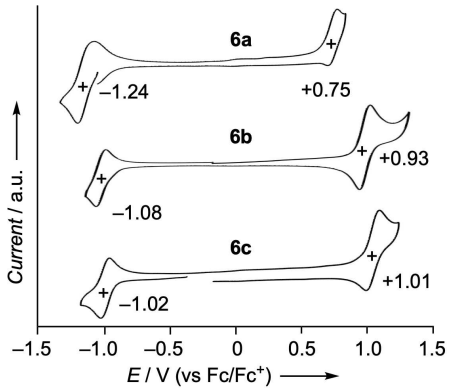

Figure 5. Cyclic voltammograms of **6a-Cl**, **6b-Cl**, and **6c-Cl**. Measured in CH_2Cl_2 with Bu_4NPF_6; scan rate = 60 mV s^{-1}. Half-wave potentials ($E_{1/2}$) vs. Fc/Fc^+ are indicated.

agreement with the optical HOMO-LUMO gaps determined by UV/vis absorption/emission spectroscopy.

The internal NH groups of the H_2TAMAP cation may be more acidic than H_2TPP and can be converted to its deprotonated form, as observed for a free base of 5-methyl-10,20-dimesityl-5,15-diazaporphyrinium salt.[24] On this basis, a $CDCl_3$ solution of **10a-Br** (ca. 0.4 mM) was treated with an equimolar amount of 1,8-diazabicyclo[5.4.0]-7-undecene (DBU), which resulted in an immediate color change from dark green to purplish red (Figure S7). We presumed that DBU deprotonated one of the inner NH groups of the H_2TAMAP cation to generate neutral HTAMAP **11a** (Scheme 3). This was further confirmed by ^{1}H NMR spectroscopy and HRMS spectrometry. The ^{1}H NMR spectrum of **11a** in $CDCl_3$ displayed four doublet signals corresponding to the pyrrolic β-protons in the range of 8.1–7.3 ppm and a broad singlet signal that represented the inner NH proton at 0.89 ppm, reflecting rather weak diatropic ring-current effects from its 18π-electron circuit (Figures S7 and S30). When an aqueous HBr solution was added to the $CDCl_3$ solution of **11a**, **10a-Br** was quantitatively regenerated. These results indicate that deprotonation and protonation between the H_2TAMAP cation (**10a-Br**) and neutral HTAMAP (**11a**) occurred reversibly.

Finally, the $^1O_2$-generating ability of **6a-PF$_6$** was studied. A decrease in the amount of 1,3-diphenylisobenzofuran (DPBF; a $^1O_2$ quencher) was observed following the irradiation of a toluene solution containing **6a-PF$_6$** and excess DPBF using a xenon lamp through a band-path filter (λ_{ex} = 540 nm; for details, see the Supporting Information). The chemically determined quantum yield of $^1O_2$ generation (Φ_Δ) was 0.77.[25] This result demonstrates the potential of the TAMAP salts as an ionic azaporphyrin photosensitizer for PDT applications.

Conclusions

In summary, we have established a new method for the synthesis of MTAMAP salts from two different dipyrrin precursors using the metal-templated annulation strategy. The MTAMAP salts exhibited Q bands that were red-shifted and intensified as well as 18π/19π- and 18π/17π-electron redox processes that were positively shifted, reflecting the pronounced electronic effect of the positive charge resulting from the inclusion of a single *meso*-nitrogen atom in the 18π-electron circuit of the porphyrin ring. The diatropic ring-current effects observed for the TAMAP cations were appreciably weaker than those observed for the TAP and TADAP dications, probably owing to the highly polarized nature of the MAP π electrons. It is worth noting that the fluorescence intensities of the ZnTAMAP salts depended on the counter anions and solvents. The present findings suggest that MTAMAP salts would be promising scaffolds for the development of new azaporphyrin-based ionic fluorophores and photosensitizers that are responsive to external stimuli, such as anionic species and solvents.

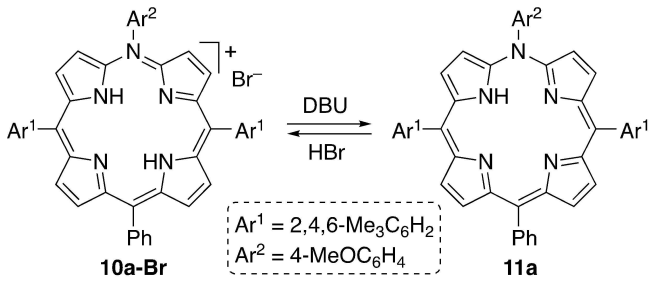

Scheme 3. Deprotonation of **10a-Br** and protonation of **11a** in $CDCl_3$.

Experimental Section

General Remarks: All melting points were recorded on a micro melting point apparatus and are uncorrected. The NMR spectra were recorded on 400 MHz and 700 MHz (Agilent and Bruker) spectrometers. The ^{1}H and ^{13}C chemical shifts are reported in ppm as relative values vs. tetramethylsilane, and the ^{19}F and ^{31}P chemical shifts are reported in ppm as relative values vs. $CFCl_3$ and H_3PO_4, respectively. High-resolution mass (HRMS) spectra were measured on a Thermo Fisher Scientific EXACTIVE spectrometer (electron spray-quadrupole). The UV-Vis absorption spectra were measured on a JASCO V-530 spectrometer, and the UV-Vis fluorescence spectra were measured on a JASCO EP-8300 spectrometer. Absolute fluorescence quantum yields were measured on a Hamamatsu Photonics Quantaurus-QY spectrometer. The IR (Attenuated Total Reflection; ATR) spectra were obtained on a JASCO FT/IR4600 spectrometer. Redox potentials and electrochemical behavior were measured at room temperature on an ALS model 650E electrochemical workstation using a glassy carbon working electrode, a platinum wire counter electrode, and an Ag/Ag^+ [0.01 M $AgNO_3$, 0.1 M Bu_4NPF_6 (MeCN)] reference electrode. Thin-layer chromatography was performed with Kieselgel 60 F254, and preparative column chromatography was performed using Silica Gel 60 spherical, neutrality. All reactions were performed under an argon or nitrogen atmosphere unless otherwise noted. Oil baths were used to heat reaction vessels, and the oil-bath temperatures are indicated in Scheme 1 and the following synthetic procedures. Compounds **1**[26] and **3**[27] were prepared according to reported procedures. Other chemicals and solvents were of reagent grade quality and used without further purification unless otherwise noted. For all the synthesis and characterization data of new compounds are reported in the Supporting Information.

X-ray Crystallographic Analysis: Single crystals of **6a-PF$_6$**·H_2O were grown from CH_2Cl_2-hexane at room temperature.

Deposition Number 2278095 (for **6a-PF$_6$**) contains the supplementary crystallographic data for this paper. These data are provided free of charge by the joint Cambridge Crystallographic Data Centre and Fachinformationszentrum Karlsruhe Access Structures service.

Selected structure parameters are as follows. $C_{56}H_{56}F_6N_5O_2PZn$, MW = 1041.39, 0.05×0.05×0.05 mm, monoclinic, $P2_1/c$, a = 21.517(3) Å, b = 14.9120(17) Å, c = 16.1439(19) Å, β = 108.556(4)°, V = 4910.6(10) Å^3, Z = 4, ρ_{calcd} = 1.409 g cm^{-3}, μ = 6.05 cm^{-1}, collected 197640, independent 11252, parameters 712, R_w = 0.1378 (all data), R_1 = 0.0492 ($I > 2.0\sigma(I)$), GOF = 1.037.

DFT Calculations: The geometries of model compounds were optimized with the density functional theory (DFT) method. The basis sets used for the optimization were 6–311G(d,p) basis set[28] for H, C, and N and the Wachters-Hay all electron basis set[29] supplemented with one f-function (exponent: 1.62) for Zn. The functional of DFT was the Becke, three-parameter, Lee-Yang-Parr (B3LYP) exchange-correlation functional.[30] The optimized geo-

metries were confirmed to be minima by vibrational analysis. The Cartesian coordinates and computed total energies of newly calculated models (**6m**$^+$, 5-HMAP$^+$, **10m**$^+$, H_2TPP, and **H_2-P1m**$^{2+}$) are summarized in Table S4. The excitation energies and oscillator strengths listed in Table S2 were computed with the time-dependent density functional theory (TD-DFT) method. The solvent effects were incorporated in both the DFT and TD-DFT calculations using the polarizable continuum model (PCM) with the integral equation formalism variant.[31] The nucleus-independent chemical shift (NICS)[32] were calculated at the Hartree-Fock level with gauge-including atomic orbitals (GIAOs) at the DFT optimized geometries. The basis set used for the NICS calculations was 6–31 + G(d).[33] The NICS values are shown in Figure S1. Anisotropy of the current-induced density (ACID) analysis[34] was performed to evaluate the aromaticity of (aza)porphines, and the current density vectors plotted on the ACID isosurfaces of 5-HMAP$^+$, porphine, and 5,15-H_2DAP^{2+} are shown in Figure S2. The solvent effect was not included in the NICS and ACID calculations. All the calculations were carried out using the Gaussian 16 suite of programs.[35]

Fluorescence Lifetime Measurements: The fluorescence lifetimes of **6a-X** were measured using a streak camera as a fluorescence detector. The excitation pulse (400 nm) was generated by taking the second harmonic pulse of the fundamental output of an amplified Ti:Sapphire laser system (Spectra Physics, Spitfire XPpro). Compounds **6a-Cl** (in MeOH), **6a-PF_6**, and **6a-NTf_2** showed single-exponential decay profiles with the lifetimes indicated in Table S3, whereas **6a-Cl** in CH_2Cl_2 displayed double exponential decays mainly dominated by the faster decay component.

Measurement of $^1O_2$ Generation Efficiency: A mixture of sensitizer (**6a-PF_6** or 5,10,15,20-tetraphenylporphyrinatozinc(II) (ZnTPP) (Abs = ca. 0.2 at irradiation wavelength), 1,3-diphenylisobenzofran (DPBF; 120 μM), and toluene (2 mL) was stirred in a quartz cell at 25 °C. Irradiation was carried out with a xenon lamp (LAX-103, Asahi Spectra). A band path filter (540 nm, band width at 0.5 peak = 10.0 nm, Asahi Spectra) was placed in the light beam path of the lamp. The consumption of DPBF was monitored at several intervals (the monitoring wavelengths are 411 nm; Figure S8). The relative $^1O_2$-generation quantum yield of **6a-PF_6** was determined by comparison with the reported value for ZnTPP (94 %).[36]

Acknowledgements

This work was supported by JSPS KAKENHI (21H05476 and 22H02061 to YM, 21 K04980 to HN) from MEXT, Japan.

Conflict of Interests

The authors declare no conflict of interest.

Data Availability Statement

The data that support the findings of this study are available in the supplementary material of this article.

Keywords: dyes/pigments · fluorescence · monoazaporphyrin · porphyrinoids · singlet oxygen

[1] a) J. Mack, N. Kobayashi, *Chem. Rev.* **2011**, *111*, 281–321; b) Y. Matano, *Chem. Rev.* **2017**, *117*, 3138–3191; c) Y. Matano, *Org. Biomol. Chem.* **2023**, *21*, 3034–3056.
[2] a) K. Ishii, N. Kobayashi in *The Porphyrin Handbook, Vol 16* (Eds.: K. M. Kadish, K. M. Smith, R. Guilard), Academic Press, San Diego, **2003**, pp. 1–42; b) H. Ogata, T. Fukuda, K. Nakai, Y. Fujimura, S. Neya, P. A. Stuzhin, N. Kobayashi, *Eur. J. Inorg. Chem.* **2004**, 1621–1629.
[3] For example, see: a) H. Shinmori, F. Kodaira, S. Matsugo, S. Kawabata, A. Osuka, *Chem. Lett.* **2005**, *34*, 322–323; b) J.-F. Longevial, A. Yamaji, D. Aggad, G. Kim, W.-X. Chia, T. Nishimura, Y. Miyake, S. Clément, J. Oh, M. Daurat, C. Nguyen, D. Kim, M. Gary-Bobo, S. Richeter, H. Shinokubo, *Chem. Commun.* **2018**, *54*, 13829–13832; c) S. Omomo, T. Sugai, M. Minoura, H. Nakano, Y. Matano, *Angew. Chem. Int. Ed.* **2018**, *57*, 3797–3800; *Angew. Chem.* **2018**, *130*, 3859–3862; d) S. Omomo, R. Fukuda, T. Miura, T. Murakami, T. Ikoma, Y. Matano, *ChemPlusChem* **2019**, *84*, 740–745; e) S. Satake, H. Shinmori, S. Kawabata, K. Sugikawa, H. Funabashi, A. Kuroda, A. Ikeda, *Org. Biomol. Chem.* **2019**, *17*, 3141–3149; f) S. Hino, S. Satake, H. Shinmori, S. Kawabata, K. Koumoto, T. Suzuki, T. Nagasaki, K. Sugikawa, R. Kawasaki, A. Ikeda, *Chem. Asian J.* **2020**, *15*, 365–370; g) L. M. A. Ali, K. Miyagawa, N. Fukui, M. Onofre, K. El Cheikh, A. Morère, S. Clément, M. Gary-Bobo, S. Richeter, H. Shinokubo, *Org. Biomol. Chem.* **2022**, *20*, 8217–8222.
[4] S. Omomo, Y. Tsuji, K. Sugiura, T. Higashino, H. Nakano, H. Imahori, Y. Matano, *ChemPlusChem* **2017**, *82*, 695–704.
[5] a) T. Nishimura, Y. Miyake, H. Shinokubo, *Chem. Lett.* **2017**, *46*, 995–997; b) T. Nishimura, T. Sakurai, H. Shinokubo, Y. Miyake, *Dalton Trans.* **2021**, *50*, 6343–6348; c) M. Nishijo, S. Mori, T. Nishimura, H. Shinokubo, Y. Miyake, *Chem. Asian J.* **2022**, *17*, e202200305.
[6] a) T. Satoh, M. Minoura, H. Nakano, K. Furukawa, Y. Matano, *Angew. Chem. Int. Ed.* **2016**, *55*, 2235–2238; *Angew. Chem.* **2016**, *128*, 2275–2278; b) K. Sudoh, T. Satoh, T. Amaya, K. Furukawa, M. Minoura, H. Nakano, Y. Matano, *Chem. Eur. J.* **2017**, *23*, 16364–16373; c) M. Mutoh, K. Sudoh, K. Furukawa, M. Minoura, H. Nakano, Y. Matano, *Asian J. Org. Chem.* **2019**, *8*, 352–355.
[7] Y. Satoh, Y. Fujita, N. Muramatsu, K. Furukawa, T. Ikoma, M. Minoura, H. Nakano, Y. Matano, *ChemPlusChem* **2021**, *86*, 1476–1486.
[8] Y. Satoh, Y. Kudoh, K. Furukawa, Y. Matano, *Org. Lett.* **2022**, *24*, 3839–3843.
[9] H. Ochiai, K. Furukawa, H. Nakano, Y. Matano, *J. Org. Chem.* **2021**, *86*, 2283–2296.
[10] β-Substituted MAPs. For example, see: a) R. L. N. Harris, A. W. Johnson, I. T. Kay, *J. Chem. Soc. C* **1966**, 22–29; b) J. Engel, A. Gossauer, A. W. Johnson, *J. Chem. Soc., Perkin Trans. 1* **1978**, 871–875; c) R. K. Pandey, K. R. Gerzevske, H. Zhou, K. M. Smith, *J. Chem. Soc., Perkin Trans. 1* **1994**, 971–977; d) J. P. Singh, L. Y. Xie, D. Dolphin, *Tetrahedron Lett.* **1995**, *36*, 1567–1570; e) S. Neya, T. Sato, T. Hoshino, *Tetrahedron Lett.* **2008**, *49*, 1613–1615; f) Y. B. Ivanova, Y. I. Chyrakhin, A. S. Semeikin, R. S. Kumeev, N. Z. Mamardashvili, *Russ. J. Gen. Chem.* **2008**, *78*, 1972–1976.
[11] Tetrabenzo-MAPs. For example, see: a) A. N. Cammidge, M. J. Cook, D. L. Hughes, F. Nekelson, M. Rahman, *Chem. Commun.* **2005**, 930–932; b) A. N. Cammidge, I. Chambrier, M. J. Cook, D. L. Hughes, M. Rahman, L. Sosa-Vargas, *Chem. Eur. J.* **2011**, *17*, 3136–3146; c) J. Mack, L. Sosa-Vargas, S. J. Coles, G. J. Tizzard, I. Chambrier, A. N. Cammidge, M. J. Cook, N. Kobayashi, *Inorg. Chem.* **2012**, *51*, 12820–12833; d) A. van As, C. C. Joubert, B. E. Buitendach, E. Erasmus, J. Conradie, A. N. Cammidge, I. Chambrier, M. J. Cook, J. C. Swarts, *Inorg. Chem.* **2015**, *54*, 5329–5341.
[12] *meso-C*-Substituted MAPs. J. H. Palmer, T. Brock-Nannestad, A. Mahammed, A. C. Durrell, D. VanderVelde, S. Virgil, Z. Gross, H. B. Gray, *Angew. Chem. Int. Ed.* **2011**, *50*, 9433–9436; *Angew. Chem.* **2011**, *123*, 9605–9608.
[13] A. Takiguchi, S. Kang, N. Fukui, D. Kim, H. Shinokubo, *Angew. Chem., Int. Ed.* **2021**, *60*, 2915–2919; *Angew. Chem.* **2021**, *133*, 2951–2955.
[14] A. Takiguchi, H. Shinokubo, *Chem. Lett.* **2021**, *51*, 590–593.
[15] S. H. H. Zaidi, K. Muthukumaran, S. Tamaru, J. S. Lindsey, *J. Org. Chem.* **2004**, *69*, 8356–8365.
[16] Demetallation of **6a-Cl** with an aqueous HCl solution was not successful, suggesting that a dry protic acid is superior to wet for demetallation of the ZnTAMAP salt.
[17] a) P. v. R. Schleyer, C. Maerker, A. Dransfeld, H. Jiao, N. J. R. van Eikema Hommes, *J. Am. Chem. Soc.* **1996**, *118*, 6317–6318; b) Z. Chen, C. S. Wannere, C. Corminboeuf, R. Puchta, P. v. R. Schleyer, *Chem. Rev.* **2005**, *105*, 3842–3888.
[18] D. Geuenich, K. Hess, F. Köhler, R. Herges, *Chem. Rev.* **2005**, *105*, 3758–3772.

[19] The calculated dipole moment of **6m**$^+$ is 5.41 D, whereas that of ZnTPP is 0 D.
[20] G. Subramanian, P. v. R. Schleyer, H. Jiao, *Organometallics* **1997**, *16*, 2362–2369.
[21] The water molecule can coordinate to the zinc center of **6a-PF$_6$** in solution, although not shown in the simplified structure of Figure . The equivalent appearance of the *ortho*-CH_3/*meta*-H signals of the mesityl groups in the ^{1}H NMR spectrum of **6a-PF$_6$** indicates that the adsorption-desorption behavior of H_2O occurred very rapidly on the NMR timescale.
[22] a) T. M. Krygowski, *J. Chem. Inf. Comput. Sci.* **1993**, *33*, 70–78; b) T. M. Krygowski, A. Ciesielski, C. W. Bird, A. Kotschy, *J. Chem. Inf. Comput. Sci.* **1995**, *35*, 203–210; c) M. K. Cyrañski, T. M. Krygowski, M. Wisiorowski, N. J. R. van Eikema Hommes, P. von R. Schleyer, *Angew. Chem. Int. Ed.* **1998**, *37*, 177–180; *Angew. Chem.* **1998**, *110*, 187–190.
[23] Redox potentials of 5,15-dimesityl-10,20-diphenylporphyrinatozinc(II)[6b] were determined. $E_{1/2} = -0.83$ V ($19\pi/18\pi$) and $+0.50$ V ($18\pi/17\pi$).
[24] W. X. Chia, M. Nishijo, S. Kang, J. Oh, T. Nishimura, H. Omori, J.-F. Longevial, Y. Miyake, D. Kim, H. Shinokubo, *Chem. Eur. J.* **2020**, *26*, 2754–2760.
[25] ZnTPP was used as a reference. W. Spiller, H. Kliesch, D. Wöhrle, S. Hackbarth, B. Röder, G. Schnurpfeil, *J. Porphyr. Phthalocyanines* **1988**, *2*, 145–158.
[26] J. K. Laha, C. Muthiah, M. Taniguchi, J. S. Lindsey, *J. Org. Chem.* **2006**, *71*, 7049–7052.
[27] K. Sudoh, T. Hatakeyama, K. Furukawa, H. Nakano, Y. Matano, *J. Porphyr. Phthalocyanines* **2018**, *22*, 542–551.
[28] R. Krishnan, J. S. Binkley, R. Seeger, J. A. Pople, *J. Chem. Phys.* **1980**, *72*, 650–654.
[29] a) A. J. H. Wachters, *J. Chem. Phys.* **1970**, *52*, 1033–1036; b) P. J. Hay, *J. Chem. Phys.* **1977**, *66*, 4377–4384; c) K. Raghavachari, G. W. Trucks, *J. Chem. Phys.* **1989**, *91*, 1062–1065.
[30] a) A. D. Becke, *J. Chem. Phys.* **1993**, *98*, 5648–5652; b) C. Lee, W. Yang, R. G. Parr, *Phys. Rev. B* **1988**, *37*, 785–789.
[31] E. Cancès, B. Mennucci, J. Tomasi, *J. Chem. Phys.* **1997**, *107*, 3032–3041.
[32] P. v. R. Schleyer, C. Maerker, A. Dransfeld, H. Jiao, N. J. R. van Eikema Hommes, *J. Am. Chem. Soc.* **1996**, *118*, 6317–6318.
[33] a) W. J. Hehre, R. Ditchfield, J. A. Pople, *J. Chem. Phys.* **1972**, *56*, 2257–2261; b) P. C. Hariharan, J. A. Pople, *Theor. Chim. Acta* **1973**, *28*, 213–222; c) T. Clark, J. Chandrasekhar, G. W. Spitznagel, P. v. R. Schleyer, *J. Comput. Chem.* **1983**, *4*, 294–301; d) V. A. Rassolov, J. A. Pople, M. A. Ratner, T. L. Windus, *J. Chem. Phys.* **1998**, *109*, 1223–1229.
[34] D. Geuenich, K. Hess, F. Köhler, R. Herges, *Chem. Rev.* **2005**, *105*, 3758–3772.
[35] *Gaussian 16, Revision C.01*; M. J. Frisch, G. W. Trucks, H. B. Schlegel, G. E. Scuseria, M. A. Robb, J. R. Cheeseman, G. Scalmani, V. Barone, G. A. Petersson, H. Nakatsuji, X. Li, M. Caricato, A. V. Marenich, J. Bloino, B. G. Janesko, R. Gomperts, B. Mennucci, H. P. Hratchian, J. V. Ortiz, A. F. Izmaylov, J. L. Sonnenberg, D. Williams-Young, F. Ding, F. Lipparini, F. Egidi, J. Goings, B. Peng, A. Petrone, T. Henderson, D. Ranasinghe, V. G. Zakrzewski, J. Gao, N. Rega, G. Zheng, W. Liang, M. Hada, M. Ehara, K. Toyota, R. Fukuda, J. Hasegawa, M. Ishida, T. Nakajima, Y. Honda, O. Kitao, H. Nakai, T. Vreven, K. Throssell, J. A. Montgomery, Jr., J. E. Peralta, F. Ogliaro, M. J. Bearpark, J. J. Heyd, E. N. Brothers, K. N. Kudin, V. N. Staroverov, T. A. Keith, R. Kobayashi, J. Normand, K. Raghavachari, A. P. Rendell, J. C. Burant, S. S. Iyengar, J. Tomasi, M. Cossi, J. M. Millam, M. Klene, C. Adamo, R. Cammi, J. W. Ochterski, R. L. Martin, K. Morokuma, O. Farkas, J. B. Foresman, D. J. Fox, Gaussian, Inc., Wallingford CT, **2019**.
[36] W. Spiller, H. Kliesch, D. Wöhrle, S. Hackbarth, B. Röder, G. Schnurpfeil, *J. Porphyr. Phthalocyanines* **1988**, *2*, 145–158.

Manuscript received: July 6, 2023
Accepted manuscript online: August 9, 2023
Version of record online: September 28, 2023